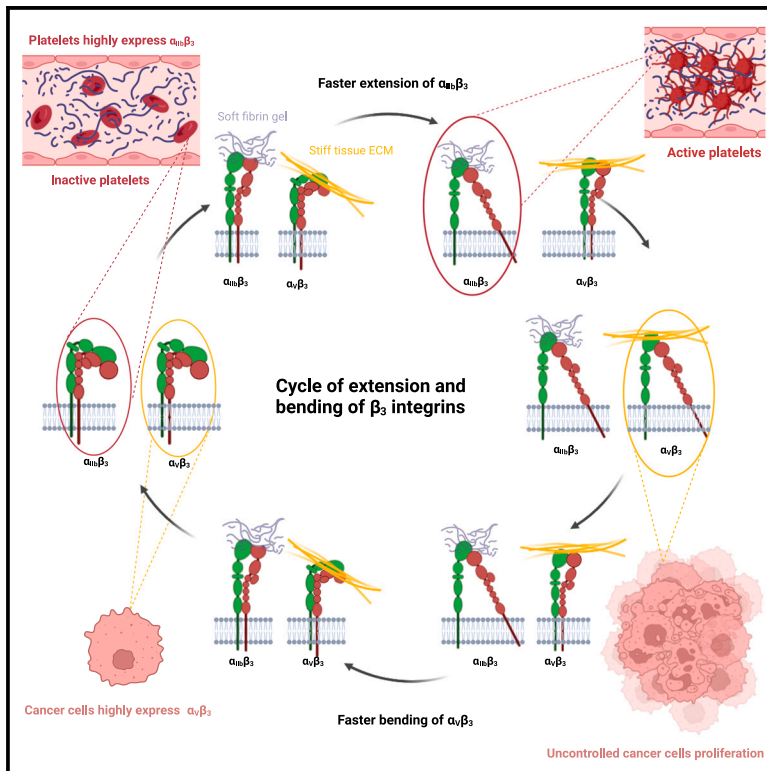


# Structure

## Conformational response of $\alpha_{IIb}\beta_3$ and $\alpha_V\beta_3$ integrins to force

### Graphical abstract



### Authors

Reza Kolasangiani,  
Khashayar Farzaniyan, Yunfeng Chen,  
Martin A. Schwartz, Tamara C. Bidone

### Correspondence

tamarabidone@sci.utah.edu

### In brief

Kolasangiani et al. investigated the effect of force on the structural dynamics of  $\alpha_{IIb}\beta_3$  and  $\alpha_V\beta_3$  integrins. They found that  $\alpha_{IIb}\beta_3$ 's higher force sensitivity and faster extension kinetics support cell spreading on soft substrates, highlighting how mechanosensitive proteins with similar structures can play diverse roles.

### Highlights

- $\alpha_{IIb}\beta_3$  promotes cell spreading on softer substrates compared to  $\alpha_V\beta_3$
- MD simulations show that  $\alpha_{IIb}\beta_3$  extends more than  $\alpha_V\beta_3$  in response to force
- Single molecule experiments show faster extension kinetics for  $\alpha_{IIb}\beta_3$  vs.  $\alpha_V\beta_3$
- Dynamic differences in  $\alpha_{IIb}\beta_3$  and  $\alpha_V\beta_3$  may explain their roles in mechanosensing

Article

# Conformational response of $\alpha_{IIb}\beta_3$ and $\alpha_V\beta_3$ integrins to force

Reza Kolasangiani,<sup>1,2</sup> Khashayar Farzanian,<sup>3</sup> Yunfeng Chen,<sup>4</sup> Martin A. Schwartz,<sup>3,5,6</sup> and Tamara C. Bidone<sup>1,2,7,8,9,\*</sup>

<sup>1</sup>Department of Biomedical Engineering, University of Utah, Salt Lake City, UT, USA

<sup>2</sup>Scientific Computing and Imaging Institute, University of Utah, Salt Lake City, UT, USA

<sup>3</sup>Yale Cardiovascular Research Center, Department of Internal Medicine (Cardiology), Yale University, New Haven, CT, USA

<sup>4</sup>Department of Biochemistry and Molecular Biology and Department of Pathology, University of Texas Medical Branch, 301 University Boulevard, Galveston, TX, USA

<sup>5</sup>Department of Cell Biology, Yale University, New Haven, CT, USA

<sup>6</sup>Department of Biomedical Engineering, School of Engineering and Applied Science, Yale University, New Haven, CT, USA

<sup>7</sup>Department of Biochemistry, University of Utah, Salt Lake City, UT, USA

<sup>8</sup>Department of Molecular Pharmaceutics, University of Utah, Salt Lake City, UT, USA

<sup>9</sup>Lead contact

\*Correspondence: [tamarabidone@sci.utah.edu](mailto:tamarabidone@sci.utah.edu)

<https://doi.org/10.1016/j.str.2024.11.016>

## SUMMARY

As major adhesion receptors, integrins transmit biochemical and mechanical signals across the plasma membrane. These functions are regulated by transitions between bent and extended conformations and modulated by force. To understand how force on integrins mediates cellular mechanosensing, we compared two highly homologous integrins,  $\alpha_{IIb}\beta_3$  and  $\alpha_V\beta_3$ . These integrins, expressed in circulating platelets vs. solid tissues, respectively, share the  $\beta_3$  subunit, bind similar ligands and have similar bent and extended conformations. Here, we report that in cells expressing equivalent levels of each integrin,  $\alpha_{IIb}\beta_3$  mediates spreading on softer substrates than  $\alpha_V\beta_3$ . These effects correlate with differences in structural dynamics of the two integrins under force. All-atom simulations show that  $\alpha_{IIb}\beta_3$  is more flexible than  $\alpha_V\beta_3$  due to correlated residue motions within the  $\alpha$  subunit domains. Single molecule measurements confirm that  $\alpha_{IIb}\beta_3$  extends faster than  $\alpha_V\beta_3$ . These results reveal a fundamental relationship between protein function and structural dynamics in cell mechanosensing.

## INTRODUCTION

Integrins are heterodimeric transmembrane receptors that mediate adhesion between cells and the extracellular matrix (ECM) or other cells and play critical roles in biological processes such as cell migration, growth, differentiation, and apoptosis, among others.<sup>1</sup> Each integrin is composed of non-covalently linked  $\alpha$  and  $\beta$  subunits, with a large extracellular domain that binds external ligands, two transmembrane helices, and two short cytoplasmic tails that connect to the cytoskeleton via accessory proteins. When integrins are simultaneously bound to a ligand and the cytoskeleton, they transmit mechanical force and biochemical signals, associated with transitions between bent and extended conformations.

Integrins are composed of several functional domains interconnected by flexible linkers. The  $\alpha$  subunit extracellular region consists of a  $\beta$ -propeller, a thigh, and two calf domains (Figure 1A). The  $\beta$  subunit extracellular region consists of a  $\beta$ -I, a hybrid, the plexin-semaphorin-integrin (PSI) domain, four cysteine-rich epidermal growth factor (EGF) modules, and the  $\beta$ -tail domain ( $\beta$ -TD) (Figure 1A). Transitions between bent and extended conformations involve changes in the relative positions of these do-

main. In bent integrins, the ligand binding site between  $\beta$ -propeller and  $\beta$ -I domains faces the plasma membrane. Additionally, the lower leg domains (Calf1 and Calf2 for the  $\alpha$  subunit; I-EGF1-4 and  $\beta$ -TD for the  $\beta$  subunit) are in contact with the upper leg domains (thigh and  $\beta$ -propeller for the  $\alpha$  subunit; PSI, hybrid, and  $\beta$ -I domains for the  $\beta$  subunit) (Figure 1A). In the extended-closed conformation, these contacts are lost and the ligand binding site between the  $\beta$ -propeller and  $\beta$ I domains is oriented away from the membrane (Figure 1B), with the  $\alpha$  and  $\beta$  subunits also laterally separated (Figure 1C).<sup>1-6</sup> Force straightens bent integrins<sup>1</sup> and helps maintain the extended states.<sup>7</sup> In cells, applying force to extended and ligand-bound integrins promotes the recruitment of intracellular adaptors, the reinforcement of the adhesion, and its elongation and growth<sup>8-11</sup> with a corresponding increase in cellular traction force, cell spreading and downstream signaling.<sup>12,13</sup> Cell spreading and traction force on soft substrates are also enhanced by point mutations or manganese ions that activate integrins.<sup>14</sup>

Integrin  $\alpha_{IIb}\beta_3$  is the primary integrin expressed on the surface of platelets and megakaryocytes.<sup>15-17</sup> In normal circulating platelets,  $\alpha_{IIb}\beta_3$  integrin is bent and inactive. Platelet activation leads to extension and activation of  $\alpha_{IIb}\beta_3$ , which

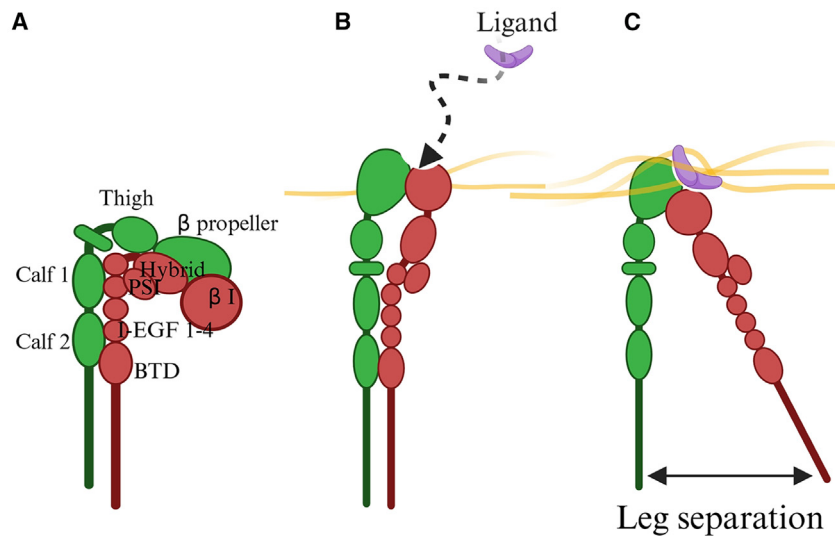


**Figure 1. Schematics of integrin in bent and extended conformations**

(A) Bent/closed conformation. The  $\alpha$  subunit (green) and the  $\beta$  subunit (red) are shown, with their domains indicated. The  $\alpha$  subunit extracellular domains are: the N-terminal  $\beta$ -propeller domain followed by the thigh domain, and two calf domains (Calf1 and Calf2). The  $\beta$  subunit extracellular domains are: the N-terminal  $\beta$ -I domain, followed by the hybrid, the plexin-semaphorin-integrin (PSI) domain, four cysteine-rich epidermal growth factor (EGF) modules (I-EGF 1–4), and the  $\beta$ -tail domain ( $\beta$ -TD). The upper legs consist of thigh and  $\beta$ -propeller domains for the  $\alpha$  subunit and PSI, hybrid, and  $\beta$ I domains for the  $\beta$  subunit. The lower legs consist of domains Calf1 and Calf2 for the  $\alpha$  subunit and I-EGF1-4 and  $\beta$ TD for the  $\beta$  subunit.

(B) Extended-close conformation of integrin with ligand approaching the ligand binding site between the  $\beta$ -propeller and  $\beta$ I domains.

(C) Extended-open conformation with ligand bound and separated legs.

facilitates binding to fibrinogen or fibrin during hemostasis.<sup>16,18,19</sup> Dysregulation of  $\alpha_{IIb}\beta_3$  integrin conformational activation results in thrombotic or bleeding disorders.<sup>20–22</sup>  $\alpha_V\beta_3$  is expressed at  $\sim 100\times$  lower levels on platelets but is abundant in adherent cell types, including endothelial, smooth muscle, and tumor cells,<sup>23–26</sup> where it promotes cell migration, growth, and survival. Both  $\alpha_{IIb}\beta_3$  and  $\alpha_V\beta_3$  are promiscuous integrins that bind a wide range of ECM proteins, especially those presenting an arginine-glycine-aspartic acid (RGD) motif, commonly referred to as the RGD motif.<sup>27</sup>

Despite their  $\sim 75\%$  sequence similarity (Figure S1), similar bent and extended conformations, and largely overlapping ligand repertoires,<sup>28–31</sup>  $\alpha_{IIb}\beta_3$  and  $\alpha_V\beta_3$  show some functional differences.<sup>18,32</sup> They exhibit differences in their ability to bind small molecules,<sup>33</sup> the gamma chain site in fibrinogen,<sup>34,35</sup> synthetic or natural peptides, and their regulation by divalent ions.<sup>36–38</sup> Expressing  $\alpha_{IIb}\beta_3$  in human melanoma cells that already express  $\alpha_V\beta_3$  increases cell adhesion, spreading, and migration.<sup>39</sup> Platelets express about 80,000  $\alpha_{IIb}\beta_3$  molecules per cell compared to a few hundred for  $\alpha_V\beta_3$ .<sup>40–42</sup> However, the structural or conformational bases for differential functions are poorly understood.

Force on integrin is due to external or internal contractility and is transmitted between the ligand-binding site and the  $\beta$  subunit cytoplasmic tail that connects to the actin cytoskeleton. Platelets use  $\alpha_{IIb}\beta_3$  to adhere, spread and exert force on very soft fibrin gels during hemostasis, while nucleated cells use  $\alpha_V\beta_3$  to adhere and migrate on stiffer interstitial tissue ECM. Differential responses of  $\alpha_{IIb}\beta_3$  and  $\alpha_V\beta_3$  to force could underlie these functional differences.<sup>43,44</sup> We therefore addressed how  $\alpha_{IIb}\beta_3$  and  $\alpha_V\beta_3$  integrins respond to force. We started with experimental analysis of cell spreading on substrates of variable rigidities, then used steered molecular dynamics simulations to evaluate structural features that underlie differential behavior. Finally, we used a biomembrane force probe to assess the unbending kinetics of the two integrins under precise control of mechanical forces. Our results, collectively, demonstrate that differential conformational dynamics and kinetics under force for  $\alpha_{IIb}\beta_3$  and  $\alpha_V\beta_3$  integrins

correlate with and likely account for differential mechanosensing by these integrins in cells.

## RESULTS

### $\alpha_{IIb}\beta_3$ allows cell spreading on soft substrates compared to $\alpha_V\beta_3$

To understand functional differences between highly homologous integrins, we examined their behaviors in mechanotransduction. Chinese hamster ovary (CHO) cells expressing equal levels of  $\alpha_{IIb}\beta_3$  or  $\alpha_V\beta_3$  (Figure S2) were seeded onto fibrinogen-coated polyacrylamide gel substrates of varying stiffness (Table 1), plus fibrinogen-coated glass as a control.<sup>45</sup> After overnight incubation to achieve full spreading, we observed the expected increase in cell area as a function of stiffness (Figure 2A); however, cells expressing  $\alpha_{IIb}\beta_3$  showed greater spreading at  $\sim 5$  kPa (Figures 2A and 2B), while spreading on stiff substrates (30 kPa) or glass was marginally higher for  $\alpha_V\beta_3$  (Figures 2A and 2B). The addition of  $Mn^{2+}$ , a well-established positive control for integrin activation, had little effect on the difference between  $\alpha_{IIb}\beta_3$  and  $\alpha_V\beta_3$  (Figure 2B).  $Mn^{2+}$  treated  $\alpha_{IIb}\beta_3$  cells spread less on substrates of  $\sim 5$  kPa compared to the cells expressing  $\alpha_{IIb}\beta_3$  in the absence of  $Mn^{2+}$  (Figure 2B), which was initially unexpected; however,  $\alpha_{IIb}\beta_3$  with bound  $Mn^{2+}$  is in an intermediate activation state,<sup>46</sup> with a slower association rate for ligands.<sup>36</sup> Taken together, these results suggest that either a lower threshold for force-dependent activation or a higher threshold for bending of integrin  $\alpha_{IIb}\beta_3$  relative to  $\alpha_V\beta_3$  mediates this effect.

### All-atom simulations of $\alpha_{IIb}\beta_3$ and $\alpha_V\beta_3$ extension-bending

We evaluated force-dependent extension and bending of  $\alpha_{IIb}\beta_3$  and  $\alpha_V\beta_3$  integrins using steered molecular dynamics (SMD) and equilibrium molecular dynamics (MD) simulations. A constant force of 66.4 pN was applied to the center of mass of the residues at the ligand binding site while holding the center of mass of the transmembrane helices fixed in the vertical direction to simulate spatial restraints from the lipid bilayer (Figure 3A). Integrin  $\alpha_{IIb}\beta_3$  extended up to  $\sim 9$  nm in 100 ns, while  $\alpha_V\beta_3$

**Table 1. Composition of polyacrylamide gels with varied stiffness for substrate preparation**

Elastic modulus (Pa)	40% acrylamide	2% bis-acrylamide	10% APS	Citrate buffer	NHS (60 $\mu\text{g/mL}$ )	TEMED	Total volume ( $\mu\text{L}$ )
490	45	7.5	20	394	33	1	500
1,551	56.3	10	20	372	42	0.8	500
5,083	84	11	20	323	62	0.8	500
9,000	84	18	20	316	63	0.8	500
13,380	84.4	25	20	308	63	0.5	500
30,027	135	37.5	20	208	100	0.5	500

The elastic modulus (Pa), acrylamide, bis-acrylamide, APS, citrate buffer, NHS, TEMED, and total volume ( $\mu\text{L}$ ) are detailed for each stiffness level, facilitating the creation of substrates used in the study. Gels were applied to glass surfaces following a specific protocol, and fibronectin was subsequently added for surface functionalization.

extended up to  $\sim 7.5$  nm (Figure 3B). Embedding the two integrins within a lipid bilayer showed a similar greater extension for  $\alpha_{11b}\beta_3$  compared to  $\alpha_V\beta_3$  (Figure S3). The number of hydrogen bonds decreased more rapidly for  $\alpha_{11b}\beta_3$ , especially after 30 ns, which coincides with the point at which  $\alpha_{11b}\beta_3$  extension surpassed that of  $\alpha_V\beta_3$  (Figure 3C). When larger forces of 166 pN and 322 pN were applied,  $\alpha_{11b}\beta_3$  consistently exhibited greater extension compared to  $\alpha_V\beta_3$  (Figure S4). Releasing the force resulted in bending for both integrins, but  $\alpha_{11b}\beta_3$  bent more slowly than  $\alpha_V\beta_3$  (Figure 3B). Specifically,  $\alpha_{11b}\beta_3$  bent approximately 1.5 nm from its extended conformation within 100 ns of equilibrium MD simulations, while  $\alpha_V\beta_3$  bent about 4.3 nm in the same time frame (Figure 3B). Accordingly, the number of hydrogen bonds for  $\alpha_V\beta_3$  remained higher than that of  $\alpha_{11b}\beta_3$  (Figure 3C). Collectively, analysis of integrin extension and bending from the SMD and equilibrium MD simulations indicates that  $\alpha_{11b}\beta_3$  exhibits greater flexibility than  $\alpha_V\beta_3$  under applied force; additionally, once extended,  $\alpha_{11b}\beta_3$  maintains its extended conformation longer than  $\alpha_V\beta_3$  (Videos S1 and S2). These results demonstrate that force has different effects on  $\alpha_{11b}\beta_3$  and  $\alpha_V\beta_3$ , enhancing extension and stabilizing the extended conformation of  $\alpha_{11b}\beta_3$  to a greater extent.

### Analysis of residue fluctuations during $\alpha_{11b}\beta_3$ and $\alpha_V\beta_3$ extension and bending

To gain insights into the force-dependent conformational pathways of integrin  $\alpha_{11b}\beta_3$  and  $\alpha_V\beta_3$ , root-mean-square displacements (RMSDs) and root-mean-square fluctuations (RMSFs) of the residues alpha carbons ( $C\alpha$ ) were calculated. During extension,  $C\alpha$  RMSDs of  $\alpha_{11b}\beta_3$  relative to its initial bent conformation increased more than that of  $\alpha_V\beta_3$ , reaching  $\sim 4$  nm compared to  $\sim 3$  nm at 100 ns of SMD (Figure 4A). In contrast, during bending, the  $C\alpha$  RMSDs of  $\alpha_{11b}\beta_3$  relative to its extended conformation was less than that of  $\alpha_V\beta_3$ , with values of  $\sim 1.1$  nm against  $\sim 1.5$  nm at 100 ns, reflecting the reduced propensity for extended  $\alpha_{11b}\beta_3$  to return to the bent state after termination of force (Figure 3B). During extension,  $\alpha_{11b}\beta_3$  exhibited per-residue RMSFs that were up to 66% higher than those of  $\alpha_V\beta_3$  (Figure 4C). The  $C\alpha$  RMSFs for  $\alpha_{11b}\beta_3$  ranged from 0.38 to 2.7 nm during extension, with an average of  $1.2 \pm 0.4$  nm (Figure 4C). In comparison,  $\alpha_V\beta_3$  showed a narrower range of  $C\alpha$  RMSFs, between 0.23 and 1.9 nm, averaging  $0.86 \pm 0.32$  nm (Figure 4C). To identify local differences in fluctuation patterns between the two integrins, we examined the residues corresponding to RMSF peaks in  $\alpha_{11b}\beta_3$  and minima in  $\alpha_V\beta_3$ . We extracted residues from  $\alpha_{11b}\beta_3$  that corresponded to

RMSF peaks with high prominence and aligned with minima of  $\alpha_V\beta_3$  within the  $\pm 10$  residues window. We used k-means clustering to group these residues (63 residues) into five distinct clusters (Table 2). Notably, 81% of these residues were located within the  $\alpha$  subunit domains Calf1-2 (34%),  $\beta$ -propeller (28%), and the  $\beta$  subunit domain  $\beta$ -I (19%).

Dynamic cross correlations among residues of the  $\beta$ -propeller domain (residues 1–452, regions a in Figure S5A), between these residues and those in the  $\beta$ -I domain (residue numbers 1118–1360, region b in Figure S5A) or with residues in Calf1-2 (residues 609–964, region c in Figure S5A) presented differences between the two integrins. During extension, the residues in these domains were more correlated in  $\alpha_{11b}\beta_3$  than  $\alpha_V\beta_3$  (Figure S5A). Conversely, during bending, residues of  $\beta$ -propeller with respect to one another (residues 1–452, regions a in Figure S5B), with respect to residues in  $\beta$ -I (residue numbers 1118–1360, region b in Figure S5B) or relative to residues in Calf1-2 (residues 609–964, region c in Figure S5B) were less correlated in  $\alpha_{11b}\beta_3$  than  $\alpha_V\beta_3$ . Hydrogen bonds and contacts between the  $\beta_3$  head (domains hybrid and  $\beta$ -I) and tail (domains  $\beta$ -TD, EGF3, and EGF4) after 30 ns of extension were higher for  $\alpha_V\beta_3$  compared to  $\alpha_{11b}\beta_3$  (Figures S6A and S7A). During bending, there were more hydrogen bonds and contacts between hybrid/ $\beta$ -I and within EGF domains in  $\alpha_{11b}\beta_3$ , possibly responsible for staying longer in an extended conformation (Figures S8B, S8H, S8I, S9B, and S9I). Additionally, in  $\alpha_V\beta_3$ ,  $\beta$ -propeller presented more molecular contacts and hydrogen bonds with both Thigh and  $\beta$ -I domains with respect to  $\alpha_{11b}\beta_3$  (Figures S6–S9). To examine whether  $\alpha_{11b}\beta_3$  and  $\alpha_V\beta_3$  integrins adopt similar conformations after the same duration following the onset of force-dependent extension and bending, we compared the  $C\alpha$  RMSDs of the integrins at different time points (i.e., 0 vs. 200 ns, 25 vs. 175 ns, 50 vs. 150 ns, and 75 vs. 125 ns). The  $\alpha_{11b}\beta_3$  and  $\alpha_V\beta_3$  integrins captured after 25 ns of extension and 25 ns of bending (corresponding to 125 ns of simulation) exhibited structural differences, as illustrated in Figure 4E (with the integrin structure from force-dependent extension shown in blue and from bending in yellow). The RMSDs for  $\alpha_{11b}\beta_3$  at the time points of 0 vs. 200 ns, 25 vs. 175 ns, and 50 vs. 150 ns were 3 nm, 2.4 nm, and 1 nm, respectively (Figure 4F). The same analysis for  $\alpha_V\beta_3$  revealed RMSDs of 0.65 nm, 0.4 nm, and 0.6 nm for extension versus bending. These results indicate that  $\alpha_{11b}\beta_3$ , when captured at 25, 50, and 75 ns after the onset of either extension or bending, consistently displayed greater differences in structure than  $\alpha_V\beta_3$ . This suggests a higher degree of structural variability in  $\alpha_{11b}\beta_3$ .

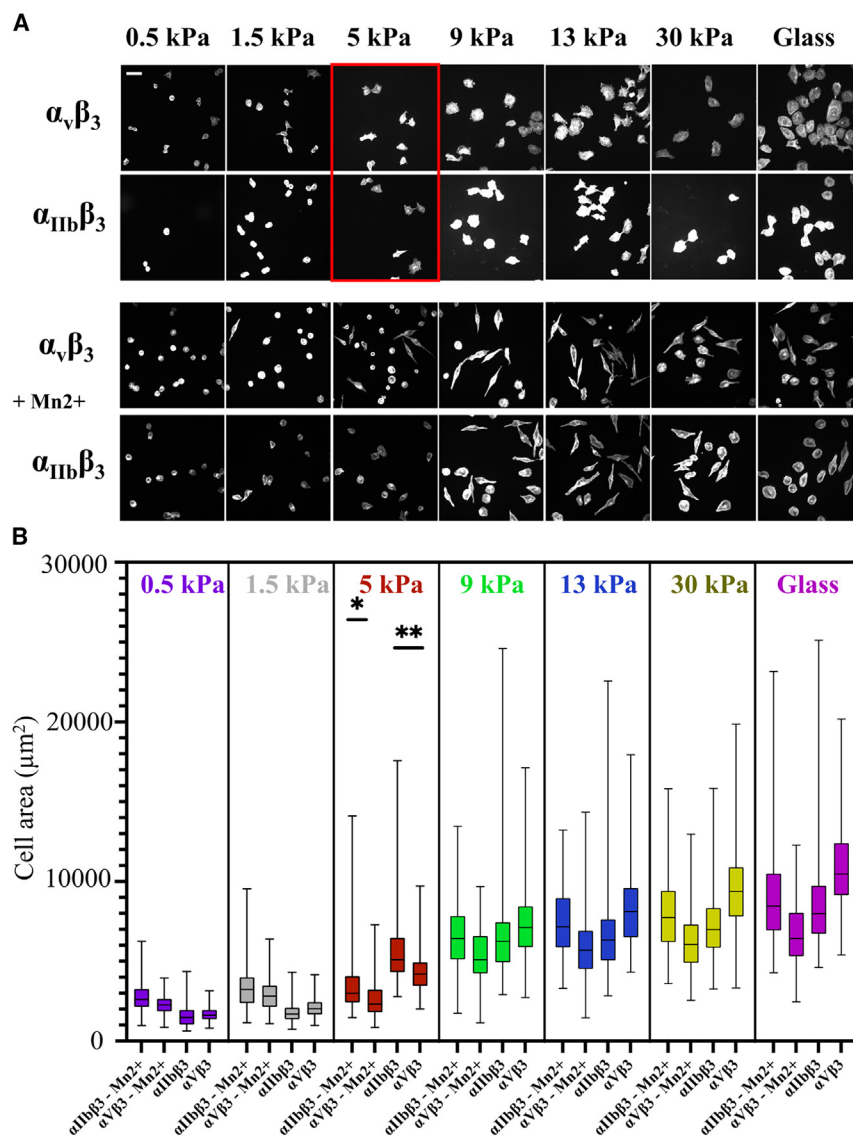


**Figure 2. Stiffness sensing via  $\alpha_{IIb}\beta_3$  and  $\alpha_V\beta_3$  integrins**

(A) CHO cells expressing equivalent levels of  $\alpha_{IIb}\beta_3$  and  $\alpha_V\beta_3$  integrins, plated on gels of indicated stiffness or glass overnight, stained for F-actin and imaged as described in Methods.

(B) Quantification of spread area per cell. Values are means  $\pm$  SEM.  $n = 199$ – $277$  cells per group from three independent experiments; \* $p < 0.0001$ , \*\* $p < 0.00001$ . Scale bar,  $100 \mu\text{m}$ .

at 100 ns of SMD related to its initial value  $r0$  (schematics in Figure 5A). For  $\alpha_{IIb}\beta_3$ , the length of the  $\alpha$  chain decreased by  $\sim 2\%$  from bent to extended, while the length of the  $\beta$  chain remained nearly constant (Figure 5B). In contrast, for  $\alpha_V\beta_3$  integrin, both the  $\alpha$  and  $\beta$  chains lengthened, with the  $\beta$  chain increasing up to  $\sim 2\%$  (Figure 5B). To understand the basis for these differences, we examined the head and leg components of the two chains separately. The shortening of  $\alpha_{IIb}$  primarily originated from the leg (Figure 5C), owing to a reduction in the distance between the centers of geometry of Calf1 and Calf2 with a maximum value of  $\sim 0.5 \text{ nm}$  (Figure 5D and Video S1). By contrast, the distance between the centers of geometry of Calf1 and Calf2 in  $\alpha_V$  remained almost constant (Figure 5D and Video S1). Collectively, these results show that the greater extension of  $\alpha_{IIb}\beta_3$  (Figure 3B) is accompanied by changes in the distance between the domains of the  $\alpha_{IIb}$  lower leg.

**Experimental observation of faster extension of integrin  $\alpha_{IIb}\beta_3$  than  $\alpha_V\beta_3$  under tensile forces**

In summary, our analysis revealed differences in structural dynamics between  $\alpha_{IIb}\beta_3$  and  $\alpha_V\beta_3$  during force-dependent extension and bending. During extension,  $\alpha_{IIb}\beta_3$  exhibited a higher degree of structural change from its bent conformation compared to  $\alpha_V\beta_3$ , with higher per-residue RMSF. The biggest differences were localized in the lower  $\alpha$  subunit, with significant but smaller contributions from the ligand-binding interface. When force was terminated,  $\alpha_{IIb}\beta_3$  maintained a more extended structure, while  $\alpha_V\beta_3$  displayed a greater propensity to adopt bent conformations like those before extension (Figure 4F).

**Integrin leg domains responsible for different extension-bending characteristics**

To assess movements between domains of  $\alpha_{IIb}\beta_3$  and  $\alpha_V\beta_3$ , we next tracked the distances between their centers of geometry during SMD and equilibrium MD simulations (Figures S10 and S11). From these distances, we summed the values for each subunit ( $\alpha$  and  $\beta$ ), which is proportional to the total length of each subunit. We then calculated the percent change in this value,  $r$ ,

In our previous work, we used a single-molecule force spectroscopy instrument named biomembrane force probe (BFP) to experimentally characterize the extension of single integrin  $\alpha_V\beta_3$  molecules both as purified molecules and on cell surfaces.<sup>47,48</sup> However, integrin  $\alpha_{IIb}\beta_3$  extension was not examined. To directly compare the extension kinetics of these integrins, we again used BFP to assess  $\alpha_{IIb}\beta_3$  integrins. A biotinylated human red blood cell (RBC) was aspirated by a micropipette to act as a force transducer (Figure 6A, left).<sup>47,48</sup> A probe bead bearing fibronectin type III module domains 9–10 (FN<sub>III9–10</sub>) was attached to the apex of the RBC via streptavidin-biotin interaction.<sup>49</sup> A platelet (which highly expresses integrin  $\alpha_{IIb}\beta_3$ ) was aspirated by an opposing micropipette (Figure 6A, right; Figure 6B) as the target, repeatedly touched to the probe bead, and then retracted (Figure 6C). Adhesion events between the probe bead and the platelet were signified by the elongation of the RBC, where the force applied on the RBC equals the force on the integrin  $\alpha_{IIb}\beta_3$ -ligand complex, which was calculated based on the RBC elongation distance and RBC spring constant. The

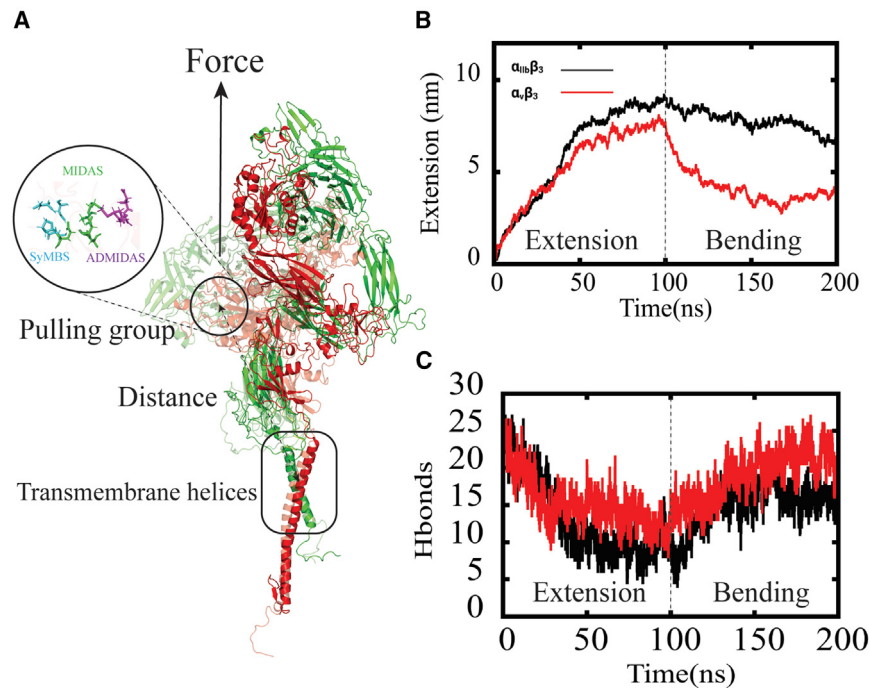


**Figure 3. Force-dependent conformational changes of  $\alpha_{IIb}\beta_3$  and  $\alpha_V\beta_3$  integrins**

(A) All-atom secondary structure representation of integrin showing force direction applied to the center of mass of the pulling group (residues: E220, S121, S123, D119, and D251 in the metal ion-dependent adhesion site or MIDAS; D217, N215, D158, and P219 in the ligand-associated metal ion binding site or LIMBS; and D126, D127, and M335 in the adjacent to MIDAS or ADMIDAS), with the  $\alpha$  chain in green and the  $\beta$  chain in red. The transparent representation corresponds to the bent integrin conformation, while the solid representation corresponds to the partially extended integrin conformation at 20 ns of the steered MD simulation. The reference group is formed by residues in the transmembrane helices: W967–W988 in the chain and V696–W715 in the  $\beta$  chain.

(B) Normalized extension vs. time plot of  $\alpha_{IIb}\beta_3$  and  $\alpha_V\beta_3$  integrins during force-dependent extension and bending. Extension is calculated as the distance between the pulling group and the reference group. Results are presented as averages between three independent replicas. The equilibrium MD simulations to simulate bending were initiated from an identical conformation, with three replicas run from this starting point to ensure consistency between simulations.

(C) Total number of hydrogen bonds within  $\alpha_{IIb}\beta_3$  and  $\alpha_V\beta_3$  integrins during extension and bending.

bead coating was titrated to reach an adhesion frequency of  $\sim 20\%$ , which allowed most binding events to be mediated by single bonds.<sup>50</sup> Antibody LM609 was added to block integrin  $\alpha_V\beta_3$  ligand binding.<sup>49</sup> As confirmed in our previous work, the binding events measured with this experimental setup were predominantly mediated by integrin  $\alpha_{IIb}\beta_3$ -ligand specific interactions.<sup>49</sup> Once an adhesion event was detected, the platelet was held at a pre-set position and clamped until integrin-ligand bond dissociation. In the clamping phase of some measurement cycles, integrin  $\alpha_{IIb}\beta_3$  extension was observed, signified by a concurrent decrease in the mean force and force fluctuation (Figures 6D and 6E), which are clearly distinguished from additional bond formation (which increases force and decreases thermal fluctuations) and dissociation of a bond from a multi-bond adhesion (which decreases force and increases thermal fluctuations).<sup>47,48,50</sup> As measured from the force drop of the BFP signals, the extension of platelet surface integrin  $\alpha_{IIb}\beta_3$  molecules was accompanied by a displacement of  $\sim 15$  nm in the integrin's ligand-binding site, in agreement with the distance the integrin headpiece moves, as estimated from the integrin structure (Figures 6F and 6G).<sup>6,47,48</sup>

The kinetics of integrin extension can be characterized using two parameters: time-to-extend ( $t_{0+}$ ), meaning the “pause” time of an integrin residing in the bent conformation before starting the extension and extending time ( $t_{sw+}$ ), meaning the duration of the extending process.<sup>48</sup> Integrin  $\alpha_{IIb}\beta_3$  showed faster unbending as force increased (Figures 6H and 6I). This is consistent with previous observations on integrins  $\alpha_L\beta_2$  and  $\alpha_V\beta_3$ , confirming a facilitating role of tensile force on integrin extension.<sup>47,48,51</sup> Although it would be ideal to compare the extension kinetics of both integrin  $\alpha_V\beta_3$  and  $\alpha_{IIb}\beta_3$  on platelet surfaces, assessing  $\alpha_V\beta_3$  on platelets is difficult due to interference from vastly

more abundant  $\alpha_{IIb}\beta_3$  ( $\sim 80,000$  vs. hundreds), while the low expression of  $\alpha_V\beta_3$  also limits the throughput of data acquisition. Thus, with a high concentration of  $10E5$  to block most  $\alpha_{IIb}\beta_3$  integrins, we only measured the unbending kinetics of platelet surface  $\alpha_V\beta_3$  (likely together with some residual events from  $\alpha_{IIb}\beta_3$ ) under a single force,  $\sim 25$  pN, which already showed much longer  $t_{0+}$  and  $t_{sw+}$  than  $\alpha_{IIb}\beta_3$  (Figures 6H and 6I). We also compared the kinetics of platelet surface integrin  $\alpha_{IIb}\beta_3$  with the published results for endothelial cell surface integrin  $\alpha_V\beta_3$  (data acquired from<sup>47</sup>), which again showed that both the  $t_{0+}$  and  $t_{sw+}$  for integrin  $\alpha_{IIb}\beta_3$  are much shorter than integrin  $\alpha_V\beta_3$  (Figures 6H and 6I).

We next examined purified integrin  $\alpha_{IIb}\beta_3$  using the same experimental setup, with the only difference being that the platelet was replaced by an integrin  $\alpha_{IIb}\beta_3$ -coated bead. Comparable to results with platelets, the extension of purified integrin  $\alpha_{IIb}\beta_3$  also involved the displacement of the integrin's ligand-binding site by  $\sim 15$  nm (Figures 6F and 6G). Interestingly, the  $t_{0+}$  of purified integrin  $\alpha_{IIb}\beta_3$  was found to be comparable to purified integrin  $\alpha_V\beta_3$  (published data acquired from a study by Chen et al.<sup>48</sup>) under all forces; however, its  $t_{sw+}$  was still much shorter than purified integrin  $\alpha_V\beta_3$ , consistent with the cell surface results (Figures 6J and 6K). Overall, the kinetics of integrin  $\alpha_{IIb}\beta_3$  extension under tensile forces is much faster than  $\alpha_V\beta_3$ , consistent with our SMD simulation.

## DISCUSSION

Integrins are central to cells' sensing the mechanical properties of their extracellular environment, but our understanding of force-induced conformational dynamics and functional consequences is rudimentary. Here, we exploit two highly

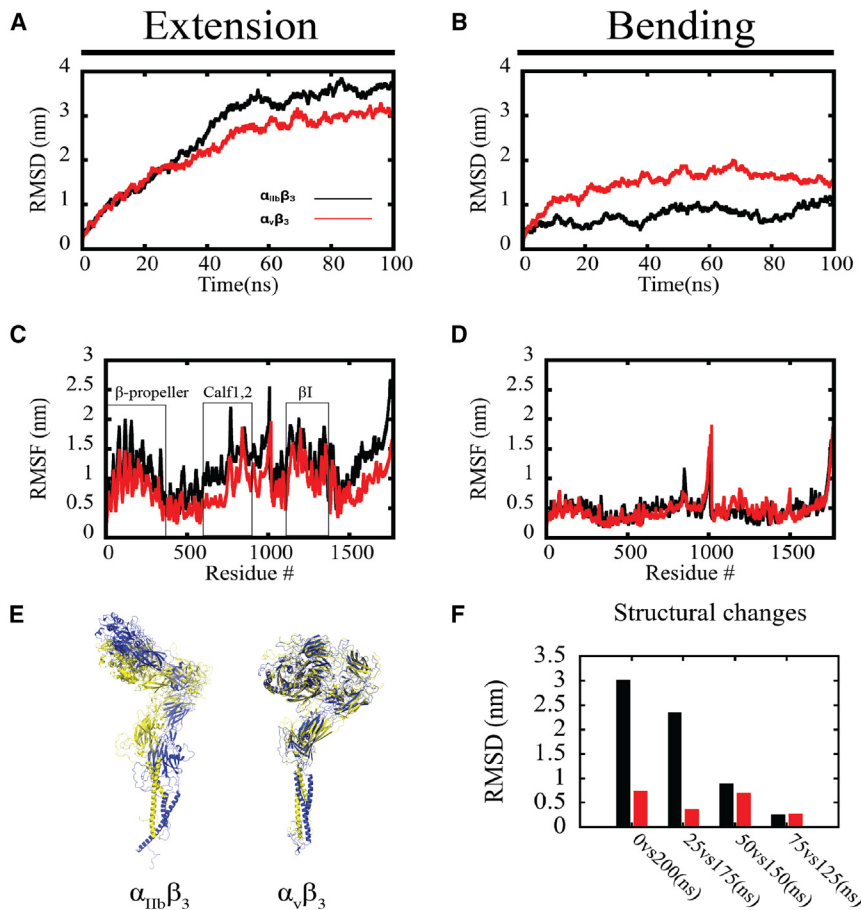


**Figure 4. Residue displacements and dynamic cross correlation (DCC) of residue pairs of  $\alpha_{IIb}\beta_3$  and  $\alpha_V\beta_3$  integrins**

(A and B) Root-mean-square displacements (RMSDs) of  $\alpha_{IIb}\beta_3$  and  $\alpha_V\beta_3$  integrin residues during extension (A) and bending (B).

(C and D) Root-mean-square fluctuations (RMSFs) of  $\alpha_{IIb}\beta_3$  and  $\alpha_V\beta_3$  integrins in the extension (C) and bending (D) phases.

(E) Structural alignment of  $\alpha_{IIb}\beta_3$  and  $\alpha_V\beta_3$  integrins to calculate the RMSDs at different extension points. Blue: integrin at a specific extension point in the extension. Yellow: integrin at a specific extension point in the bending.

(F) RMSDs of integrin at the same extension point compared between the extension and bending phases.

related integrins to address the relationship between mechanosensing functions and structural dynamics. Both integrins transition between bent and extended conformations to regulate cell adhesion and signaling. The dynamic equilibrium between these states is determined by biochemical and mechanical signals from the external environment and internal processes.<sup>47,52–54</sup> Initial and final states of integrin  $\alpha_{IIb}\beta_3$  and  $\alpha_V\beta_3$  conformational activation are extraordinarily similar, as are their ligand repertoires and properties,<sup>28–31</sup> suggesting that force-regulated dynamics should also be similar. However, our results demonstrate that substrate stiffness sensing through these integrins is quantitatively different, and that single integrin conformational dynamics, assessed both computationally and experimentally, show corresponding differences. These differences correlate well with their distinct functional activities, where  $\alpha_{IIb}\beta_3$  mediates platelet interactions with very soft fibrin gels, whereas  $\alpha_V\beta_3$  mediates nucleated cell adhesion and movement on tissue ECM.<sup>18,32</sup>

propagate motion while maintaining functional domains as cohesive, rigid units (Figure S5). By contrast,  $\alpha_V\beta_3$  was less flexible and presented reduced residue fluctuations under force (Figure 4). In the bending phase, however,  $\alpha_{IIb}\beta_3$  had less tendency to bend and stayed longer in the open conformation (Figure 3B). These findings thus explain how  $\alpha_{IIb}\beta_3$  and  $\alpha_V\beta_3$  integrins, despite their similar sequences, structures and ligand binding repertoires, respond differently to force so that platelets vs. nucleated cells can function in mechanically distinct environments.

We initially compared the responses to force of  $\alpha_{IIb}\beta_3$  and  $\alpha_V\beta_3$  integrins using the classic stiffness sensing assay as a readout, which prior studies indicated involves force-dependent changes in integrin affinity.<sup>14,55</sup> Examination in one cell type (CHO cells) was crucial for a consistent and well-controlled comparison. Stiffness sensing curves revealed a leftward shift for  $\alpha_{IIb}\beta_3$ , with greater spreading at intermediate stiffness levels compared to  $\alpha_V\beta_3$ . This difference

**Table 2. K-means clustering performed on RMSFs of integrins**

Cluster1	Cluster 2	Cluster 3	Cluster 4	Cluster 5
108, 200, 546, 686, 1310	764, 1005, <b>1317, 337, 791, 847, 81, 118, 157, 767, 1189, 339, 605, 849, 48, 794, 1010, 161, 771, 796, 1140, 53, 125, 345, 486</b>	<b>37, 148, 595, 839, 885, 887, 929, 1126</b>	887, 1001, <b>1313, 690, 842, 932, 76, 551, 599, 844</b>	856, <b>1197, 127, 166, 348, 858, 906, 1018, 1144, 1199, 1269, 1296, 1330, 1356, 1394</b>

Residues from the Calf1-2,  $\beta$ -propeller, and  $\beta$ I domains are represented in italics, bold, and bold italics, respectively.

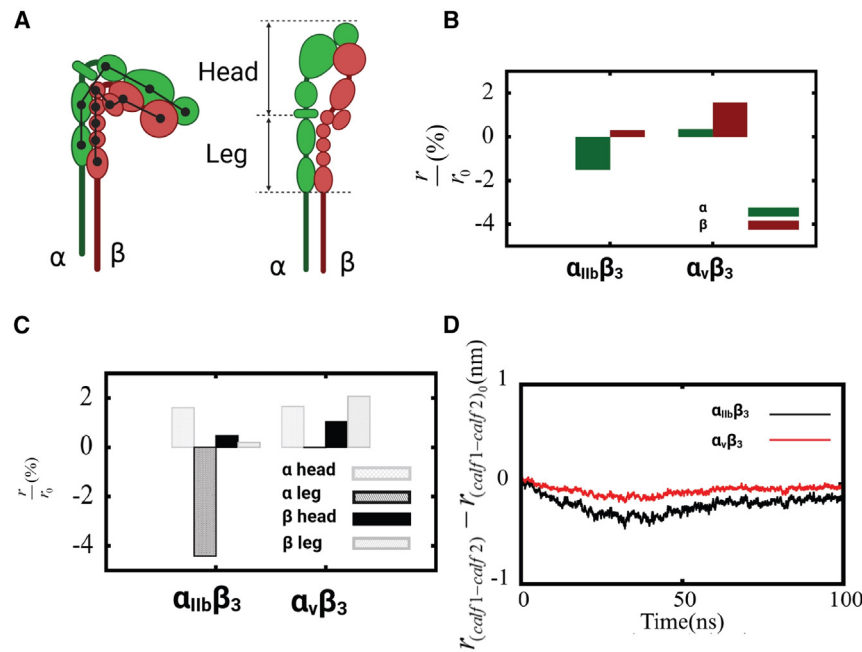


**Figure 5. Deformation of integrin chains during force-dependent extension-bending cycle**

(A) Cartoon representation of integrin in the bent and extended conformations with head and leg parts indicated. The calculation of sum of distances between the center of geometry of consecutive domains is shown in the bent conformation.

(B) Change in the length of each chain compared to their initial value.

(C) Change in head and leg part length (calculated by adding the distances between the center of geometry of consecutive domains in the head and leg part of each chain) compared to their initial value.

(D) Change in the distance between Calf1-Calf2 domains compared to the initial values in extension.

persisted in  $Mn^{2+}$  conditions. These results suggest that  $\alpha_{IIb}\beta_3$  is more prone to activation under force compared to  $\alpha_V\beta_3$  (Figure 2).

Understanding these observations requires analyzing the effects of force on the conformation of  $\alpha_{IIb}\beta_3$  and  $\alpha_V\beta_3$  integrins. However, experimentally monitoring dynamic changes in integrin conformation in cells during adhesion assembly on substrates with different rigidities is not feasible. Therefore, we employed atomistic MD simulations to evaluate integrin extension under force. SMD simulations enabled us to directly apply a constant force on the residues interacting with a ligand between the  $\alpha$  and  $\beta$  subunits of integrin. Furthermore, by releasing the force after extension and conducting unbiased MD, we assessed the relaxation of the extended conformations. Notably,  $\alpha_{IIb}\beta_3$  and  $\alpha_V\beta_3$  integrins exhibited different conformational dynamics, with  $\alpha_{IIb}\beta_3$  demonstrating greater extension under force (Figure 3B) and slower bending after releasing the force (Figure 3B). These differences emerged from different fluctuations (Figure 3) and motional correlations between residues (Figure S5) and domain movements (Figures 5, S10, and S11).  $\alpha_{IIb}\beta_3$  showed higher residue fluctuations in extension compared to  $\alpha_V\beta_3$  (Figures 4A–4D), along with a greater effect of force on inter-domain distances in the lower legs (Figure 5). In contrast,  $\alpha_V\beta_3$ , with less flexibility in extension, displayed smaller variations in inter-domain distances (Figure 5). This differential rigidity may explain the varying cell spread areas and their different functions in mechanically distinct environments.

Previous studies evaluated the relationship between residue motions and protein flexibility using molecular modeling and simulations, forming the basis for techniques like elastic network modeling and normal mode analysis.<sup>56</sup> Increasing the magnitude of residue fluctuations can decrease protein flexibility because these motions can restrict the protein's ability to adopt alternative conformations. However, in the case of  $\alpha_{IIb}\beta_3$  and  $\alpha_V\beta_3$  integ-

rins, the greater fluctuations of  $\alpha_{IIb}\beta_3$  residues (RMSFs) compared to  $\alpha_V\beta_3$  (Figure 4) in extension promoted a more dynamic and adaptable protein structure. This is because the residues' highly positive and negatively correlated motions maintain domains as rigid blocks that propagate structural changes over long distances (Figure S5).

Using the BFP, we verified that integrin  $\alpha_V\beta_3$  exhibits slower kinetics of extension under tension compared to  $\alpha_{IIb}\beta_3$ , both in purified forms and on cell surfaces, as reflected by its longer extending time ( $t_{sw+}$ ) (Figure 6). BFP allows the evaluation of bending and unbending conformational changes of a single integrin and directly assesses how its physiological function and molecular structure are coupled at the single-molecule level.<sup>47,51,57</sup> The BFP results for  $\alpha_{IIb}\beta_3$  and  $\alpha_V\beta_3$  are consistent with the extension-time plot provided by our MD simulations (Figure 3) and with the higher root-mean-square displacements (RMSDs) and greater fluctuations of  $\alpha_{IIb}\beta_3$  residues (RMSFs) compared to  $\alpha_V\beta_3$  (Figures 4C and 4D). The molecular differences between  $\alpha_{IIb}\beta_3$  and  $\alpha_V\beta_3$  integrins under force also correlate with differences in cell mechanosensing mediated by the two integrins (Figure 1).

The differences in the extension and bending of the two integrins might be responsible for controlling integrin function in the context of distinct requirements for platelets vs. adherent tissue cells. The more sensitive response of  $\alpha_{IIb}\beta_3$  to softer substrates may underlie the requirement for platelets to interact with and apply force to very soft fibrin clots. Additionally, the faster response of  $\alpha_{IIb}\beta_3$  conformational dynamics to force could be crucial for rapid hemostasis in vascular injury.<sup>58–61</sup> In contrast, the slower response of  $\alpha_V\beta_3$  to mechanical stimuli may be associated with the slower spreading and migration processes by adherent cells expressing  $\alpha_V\beta_3$  interacting with stiffer tissue extracellular matrices. Overall, this integrated experimental and computational study lays the groundwork for understanding more generally how mechanosensitive proteins with structural and conformational similarities can exhibit diverse functional roles across a spectrum of cell types, relevant for many cellular and tissue biophysics fields in physiology and diseases.

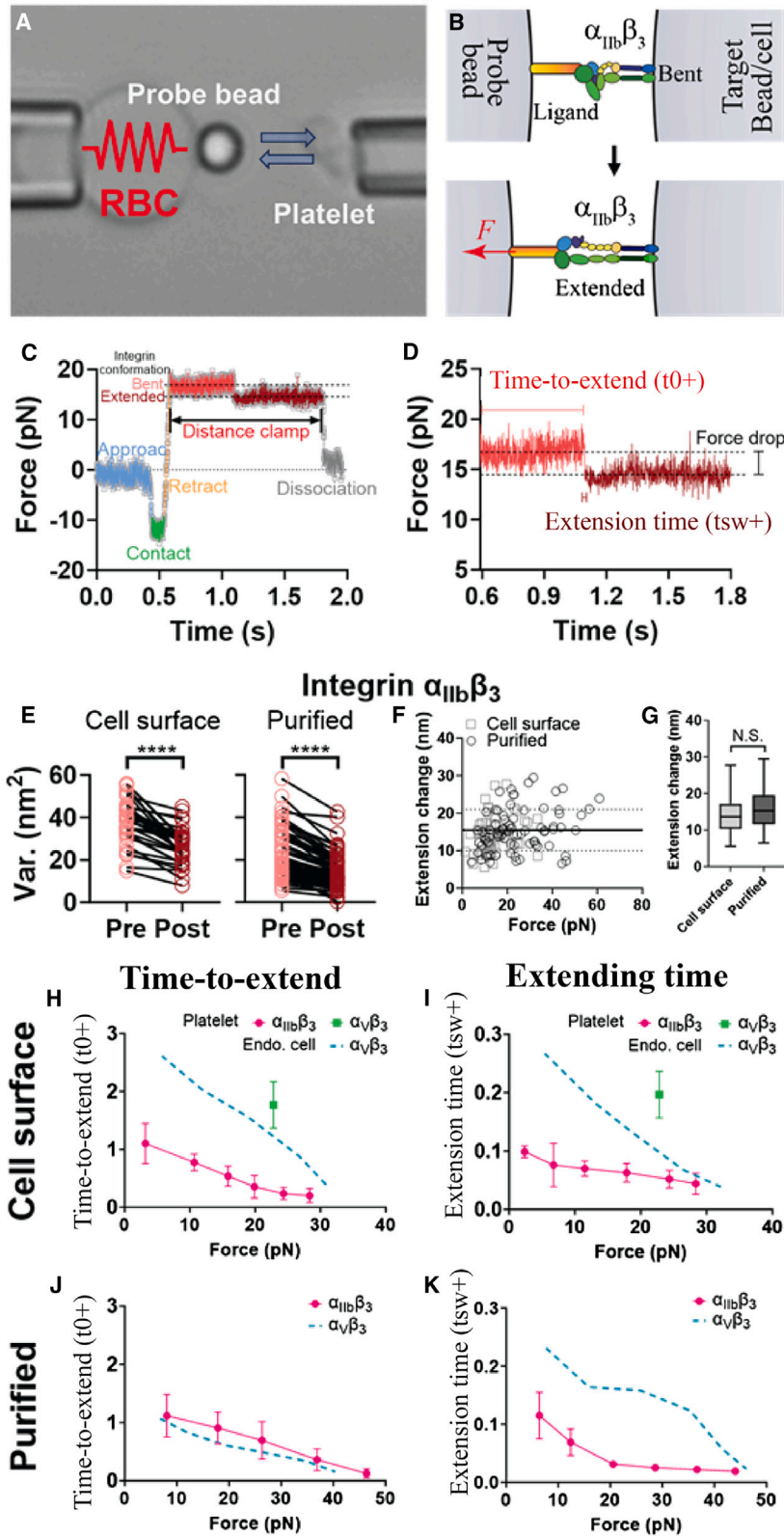


**Figure 6. Experimentally assessing kinetics of integrin  $\alpha_{IIb}\beta_3$  and  $\alpha_V\beta_3$  unbending conformational changes**

(A) Experimental setup of biomembrane force probe. (B) Illustration of the experimental design. A ligand on the probe bead engages an integrin molecule on the target bead or cell surface, and the ensuing retraction of the probe bead applies pulling force on the molecular complex and facilitates the integrin to unbend. (C) Representative BFP force vs. time trace showing different phases of a test cycle and an unbending event of purified integrin  $\alpha_{IIb}\beta_3$  in the position-clamp phase. (D) Zoom-in of the position-clamp phase in (C), with definitions of time-to-unbend, unbending time and force drop annotated. Dashed lines in (C) and (D): average clamping force when the integrin is in the bent (upper) and extended (lower) conformation, respectively. (E) Variance of pre- and post-unbending BFP signal in the purified system (left) and cell surface system (right). \*\*\*\* $p < 0.0001$ , assessed by paired sample t test. (F) Scatterplot of purified and cell surface integrin  $\alpha_{IIb}\beta_3$  unbending extension change. Solid and dashed lines: mean  $\pm$  SD. (G) Box and whisker plots of purified and cell surface integrin  $\alpha_{IIb}\beta_3$  unbending extension change. N.S., not significant, assessed by t test. (H–K) Time-to-extend ( $t_{0+}$ ) (H and J) and extension time ( $t_{sw+}$ ) (I and K) of platelet surface (H and I) and purified (J and K) integrin  $\alpha_{IIb}\beta_3$  (mean  $\pm$  SEM) and platelet surface (mean  $\pm$  SEM) and endothelial cell surface (mean; from previous publication)  $\alpha_V\beta_3$  (H and I) unbending events vs. force.

### RESOURCE AVAILABILITY

#### Lead contact

Further information and requests for resources should be directed to and will be fulfilled by the lead contact, Tamara C. Bidone ([tamarabidone@sci.utah.edu](mailto:tamarabidone@sci.utah.edu)).

#### Materials availability

All materials used in this study will be made available upon request.

#### Data and code availability

- All data reported in this paper will be shared by the [lead contact](#) upon request.
- Full-length all-atom structures of integrin  $\alpha_V\beta_3$  and  $\alpha_{IIb}\beta_3$ , MD simulation trajectories, and analysis scripts are publicly available as of the date of publication available on GitHub ([https://github.com/tamarabidone/alphaV\\_vs\\_alphaIIb](https://github.com/tamarabidone/alphaV_vs_alphaIIb)).
- Any additional information required to reanalyze the data reported in this paper is available from the [lead contact](#) upon request

### ACKNOWLEDGMENTS

This work was supported by the National Institutes of Health, National Institute of General Medical Sciences grant number 1R35GM147491-01, to T.C.B. and by the National Science Foundation, grant number 2044294, to T.C.B. and M.A.S. Also, single molecule experiment was supported by National Institutes of Health, National Heart, Lung, and Blood Institute R00-HL153678 (Y.C.), and National Institute on Aging, The Claude D. Pepper Older Americans Independence Center Award P30-AG024832 (Y.C.). Computer time was provided by the Scientific Computing and Imaging Institute and the Center for High Performance Computing at the University of Utah. Antibody 7H2 to integrin  $\beta_3$  was provided by the Developmental Studies Hybridoma Bank.

### AUTHOR CONTRIBUTIONS

Conceptualization: T.C.B. and M.A.S.; methodology: T.C.B., R.K., Y.C., and K.F.; formal analysis: R.K., Y.C., and K.F.; investigation: R.K., Y.C., and K.F.; resources: M.A.S., T.C.B., and Y.C.; data curation: R.K., Y.C., and K.F.; writing – original draft: R.K.; writing – review & editing: R.K., K.F., Y.C., M.A.S., and T.C.B.; supervision: T.C.B.; project administration: T.C.B.; funding acquisition: T.C.B., M.A.S., and Y.C.

### DECLARATION OF INTERESTS

The authors declare no competing interests.

### DECLARATION OF GENERATIVE AI AND AI-ASSISTED TECHNOLOGIES IN THE WRITING PROCESS

During the preparation of this work, the authors used ChatGPT-4 to improve language and readability. The use of ChatGPT-4 was supervised by the authors to ensure that the contribution met academic standards. After using this tool, the authors reviewed and edited the content as needed and take full responsibility for the content of the publication.

### STAR★METHODS

Detailed methods are provided in the online version of this paper and include the following:

- [KEY RESOURCES TABLE](#)
- [EXPERIMENTAL MODEL AND STUDY PARTICIPANT DETAILS](#)
  - Cell lines
- [METHOD DETAILS](#)
  - Cell culture and transfection
  - Substrate preparation
  - Cell immunostaining and quantification

- Reconstruction of missing residues
- All-atom molecular dynamics simulations of  $\alpha_{IIb}\beta_3$  and  $\alpha_V\beta_3$  extension and bending
- Energy minimization and equilibration steps
- Steered molecular dynamics simulations and equilibrium molecular dynamics of  $\alpha_{IIb}\beta_3$  and  $\alpha_V\beta_3$  integrins
- Membrane-embedded  $\alpha_{IIb}\beta_3$  and  $\alpha_V\beta_3$  simulations
- Structural and residue-based fluctuations analysis using RMSD and RMSF
- Integrin residues motions analysis using Dynamic cross correlation
- Biomembrane force probe setup, preparation, and experiment
- Red blood cell and glass bead preparation
- Platelet isolation
- Biomembrane force probe setup, preparation and experiment
- [QUANTIFICATION AND STATISTICAL ANALYSIS](#)

### SUPPLEMENTAL INFORMATION

Supplemental information can be found online at <https://doi.org/10.1016/j.str.2024.11.016>.

Received: May 7, 2024

Revised: October 9, 2024

Accepted: November 25, 2024

Published: December 19, 2024

### REFERENCES

1. Kolasangiani, R., Bidone, T.C., and Schwartz, M.A. (2022). Integrin Conformational Dynamics and Mechanotransduction. *Cells* **11**, 3584.
2. Takagi, J., Petre, B.M., Walz, T., and Springer, T.A. (2002). Global conformational rearrangements in integrin extracellular domains in outside-in and inside-out signaling. *Cell* **110**, 599–611.
3. Takagi, J., Strokovich, K., Springer, T.A., and Walz, T. (2003). Structure of integrin  $\alpha_5\beta_1$  in complex with fibronectin. *The EMBO journal* **22**, 4607–4615.
4. Nishida, N., Xie, C., Shimaoka, M., Cheng, Y., Walz, T., and Springer, T.A. (2006). Activation of leukocyte  $\beta_2$  integrins by conversion from bent to extended conformations. *Immunity* **25**, 583–594.
5. Schumacher, S., Dedden, D., Nunez, R.V., Matoba, K., Takagi, J., Biertümpfel, C., and Mizuno, N. (2021). Structural insights into integrin  $\alpha_5\beta_1$  opening by fibronectin ligand. *Sci. Adv.* **7**, eabe9716.
6. Tong, D., Soley, N., Kolasangiani, R., Schwartz, M.A., and Bidone, T.C. (2023). Integrin  $\alpha_{IIb}\beta_3$  intermediates: From molecular dynamics to adhesion assembly. *Biophys. J.* **122**, 533–543.
7. Jin, M., Andricioaei, I., and Springer, T.A. (2004). Conversion between three conformational states of integrin I domains with a C-terminal pull spring studied with molecular dynamics. *Structure* **12**, 2137–2147.
8. Wolfenson, H., Lavelin, I., and Geiger, B. (2013). Dynamic regulation of the structure and functions of integrin adhesions. *Dev. Cell* **24**, 447–458.
9. Jansen, K., Atherton, P., and Ballestrem, C. (2017). *Mechanotransduction at the Cell-Matrix Interface* (Elsevier), pp. 75–83.
10. Kechagia, J.Z., Ivaska, J., and Roca-Cusachs, P. (2019). Integrins as biomechanical sensors of the microenvironment. *Nat. Rev. Mol. Cell Biol.* **20**, 457–473.
11. Case, L.B., and Waterman, C.M. (2015). Integration of actin dynamics and cell adhesion by a three-dimensional, mechanosensitive molecular clutch. *Nat. Cell Biol.* **17**, 955–963.
12. Carisey, A., Tsang, R., Greiner, A.M., Nijenhuis, N., Heath, N., Nazgiewicz, A., Kemkemer, R., Derby, B., Spatz, J., and Ballestrem, C. (2013). Vinculin regulates the recruitment and release of core focal adhesion proteins in a force-dependent manner. *Curr. Biol.* **23**, 271–281.
13. Elosegui-Artola, A., Bazellières, E., Allen, M.D., Andreu, I., Oria, R., Sunyer, R., Gomm, J.J., Marshall, J.F., Jones, J.L., Trepats, X., and Roca-Cusachs, P.

- P. (2014). Rigidity sensing and adaptation through regulation of integrin types. *Nat. Mater.* *13*, 631–637.
14. Driscoll, T.P., Bidone, T.C., Ahn, S.J., Yu, A., Groisman, A., Voth, G.A., and Schwartz, M.A. (2021). Integrin-based mechanosensing through conformational deformation. *Biophys. J.* *120*, 4349–4359.
  15. Gao, D., Sun, C.W., Woodley, A.B., and Dong, J.-f. (2023). Clot Retraction and Its Correlation with the Function of Platelet Integrin  $\alpha IIb\beta_3$ . *Biomedicines* *11*, 2345.
  16. Ma, Y.Q., Qin, J., and Plow, E.F. (2007). Platelet integrin  $\alpha IIb\beta_3$ : activation mechanisms. *J. Thromb. Haemost.* *5*, 1345–1352.
  17. Bury, L., Malara, A., Gresele, P., and Balduini, A. (2012). Outside-in signaling generated by a constitutively activated integrin  $\alpha IIb\beta_3$  impairs proplatelet formation in human megakaryocytes. *PLoS One* *7*, e34449.
  18. Huang, J., Li, X., Shi, X., Zhu, M., Wang, J., Huang, S., Huang, X., Wang, H., Li, L., Deng, H., et al. (2019). Platelet integrin  $\alpha IIb\beta_3$ : signal transduction, regulation, and its therapeutic targeting. *J. Hematol. Oncol.* *12*, 26.
  19. Bledzka, K., Qin, J., and Plow, E.F. (2019). Integrin  $\alpha IIb\beta_3$  (Platelets), pp. 227–241.
  20. Zou, J., Swieringa, F., de Laat, B., de Groot, P.G., Roest, M., and Heemskerk, J.W.M. (2022). Reversible platelet integrin  $\alpha IIb\beta_3$  activation and thrombus instability. *Int. J. Mol. Sci.* *23*, 12512.
  21. Durrant, T.N., van den Bosch, M.T., and Hers, I. (2017). Integrin  $\alpha IIb\beta_3$  outside-in signaling. *Blood* *130*, 1607–1619.
  22. Fullard, J.F. (2004). The role of the platelet glycoprotein IIb/IIIa in thrombosis and haemostasis. *Curr. Pharm. Des.* *10*, 1567–1576.
  23. Tadokoro, S., Tomiyama, Y., Honda, S., Kashiwagi, H., Kosugi, S., Shiraga, M., Kiyoi, T., Kurata, Y., and Matsuzawa, Y. (2002). Missense mutations in the  $\beta_3$  subunit have a different impact on the expression and function between  $\alpha IIb\beta_3$  and  $\alpha V\beta_3$ . *Blood* *99*, 931–938.
  24. Soldi, R., Mitola, S., Strasly, M., Defilippi, P., Tarone, G., and Bussolino, F. (1999). Role of  $\alpha V\beta_3$  integrin in the activation of vascular endothelial growth factor receptor-2. *The EMBO journal* *18*, 882–892.
  25. Antonov, A.S., Kolodgie, F.D., Munn, D.H., and Gerrity, R.G. (2004). Regulation of macrophage foam cell formation by  $\alpha V\beta_3$  integrin: potential role in human atherosclerosis. *Am. J. Pathol.* *165*, 247–258.
  26. Rubartelli, A., Poggi, A., and Zocchi, M.R. (1997). The selective engulfment of apoptotic bodies by dendritic cells is mediated by the  $\alpha V\beta_3$  integrin and requires intracellular and extracellular calcium. *Eur. J. Immunol.* *27*, 1893–1900.
  27. Hu, D.D., Hoyer, J.R., and Smith, J.W. (1995).  $Ca^{2+}$  Suppresses Cell Adhesion to Osteopontin by Attenuating Binding Affinity for Integrin  $\alpha V\beta_3$ . *J. Biol. Chem.* *270*, 9917–9925.
  28. Xiong, J.-P., Stehle, T., Zhang, R., Joachimiak, A., Frech, M., Goodman, S.L., and Arnaout, M.A. (2002). Crystal structure of the extracellular segment of integrin  $\alpha V\beta_3$  in complex with an Arg-Gly-Asp ligand. *Science* *296*, 151–155.
  29. Bennett, J.S. (2005). Structure and function of the platelet integrin  $\alpha IIb\beta_3$ . *J. Clin. Invest.* *115*, 3363–3369.
  30. Xiao, T., Takagi, J., Collier, B.S., Wang, J.-H., and Springer, T.A. (2004). Structural basis for allostery in integrins and binding to fibrinogen-mimetic therapeutics. *Nature* *432*, 59–67.
  31. Xiong, J.-P., Stehle, T., Diefenbach, B., Zhang, R., Dunker, R., Scott, D.L., Joachimiak, A., Goodman, S.L., and Arnaout, M.A. (2001). Crystal structure of the extracellular segment of integrin  $\alpha V\beta_3$ . *Science* *294*, 339–345.
  32. Boettiger, D., Lynch, L., Blystone, S., and Huber, F. (2001). Distinct Ligand-binding Modes for Integrin  $\alpha V\beta_3$ -Mediated Adhesion to Fibronectin versus Vitronectin. *J. Biol. Chem.* *276*, 31684–31690.
  33. Blue, R., Murcia, M., Karan, C., Jirousková, M., and Collier, B.S. (2008). Application of high-throughput screening to identify a novel  $\alpha IIb$ -specific small-molecule inhibitor of  $\alpha IIb\beta_3$ -mediated platelet interaction with fibrinogen. *Blood* *111*, 1248–1256.
  34. Smith, J.W., Ruggeri, Z.M., Kunicki, T.J., and Cheresch, D.A. (1990). Interaction of integrins alpha v beta 3 and glycoprotein IIb-IIIa with fibrinogen. Differential peptide recognition accounts for distinct binding sites. *J. Biol. Chem.* *265*, 12267–12271.
  35. Cheresch, D.A., Berliner, S.A., Vicente, V., and Ruggeri, Z.M. (1989). Recognition of distinct adhesive sites on fibrinogen by related integrins on platelets and endothelial cells. *Cell* *58*, 945–953.
  36. Smith, J.W., Piotrowicz, R.S., and Mathis, D. (1994). A mechanism for divalent cation regulation of beta 3-integrins. *J. Biol. Chem.* *269*, 960–967.
  37. Yan, B., Hu, D.D., Knowles, S.K., and Smith, J.W. (2000). Probing chemical and conformational differences in the resting and active conformers of platelet integrin  $\alpha IIb\beta_3$ . *J. Biol. Chem.* *275*, 7249–7260.
  38. Ahrens, I.G., Moran, N., Aylward, K., Meade, G., Moser, M., Assefa, D., Fitzgerald, D.J., Bode, C., and Peter, K. (2006). Evidence for a differential functional regulation of the two  $\beta_3$ -integrins  $\alpha V\beta_3$  and  $\alpha IIb\beta_3$ . *Exp. Cell Res.* *312*, 925–937.
  39. Bennett, J.S., Berger, B.W., and Billings, P.C. (2009). The structure and function of platelet integrins. *J. Thromb. Haemost.* *7*, 200–205.
  40. Felding-Habermann, B., O’Toole, T.E., Smith, J.W., Fransvea, E., Ruggeri, Z.M., Ginsberg, M.H., Hughes, P.E., Pampori, N., Shattil, S.J., Saven, A., and Mueller, B.M. (2001). Integrin activation controls metastasis in human breast cancer. *Proc. Natl. Acad. Sci. USA* *98*, 1853–1858.
  41. Lavergne, M., Janus-Bell, E., Schaff, M., Gachet, C., and Mangin, P.H. (2017). Platelet integrins in tumor metastasis: do they represent a therapeutic target? *Cancers* *9*, 133.
  42. Li, S., Sampson, C., Liu, C., Piao, H.-I., and Liu, H.-X. (2023). Integrin signaling in cancer: bidirectional mechanisms and therapeutic opportunities. *Cell Commun. Signal.* *21*, 266.
  43. Mierke, C.T. (2013). The integrin alpha v beta 3 increases cellular stiffness and cytoskeletal remodeling dynamics to facilitate cancer cell invasion. *New J. Phys.* *15*, 015003.
  44. Podolnikova, N.P., Yermolenko, I.S., Fuhrmann, A., Lishko, V.K., Magonov, S., Bowen, B., Enderlein, J., Podolnikov, A.V., Ros, R., and Ugarova, T.P. (2010). Control of integrin  $\alpha IIb\beta_3$  outside-in signaling and platelet adhesion by sensing the physical properties of fibrin (ogen) substrates. *Biochemistry* *49*, 68–77.
  45. Aratyn-Schaus, Y., Oakes, P.W., Stricker, J., Winter, S.P., and Gardel, M.L. (2010). Preparation of complaint matrices for quantifying cellular contraction. *J. Vis. Exp.* 2173.
  46. Kamata, T., Handa, M., Sato, Y., Ikeda, Y., and Aiso, S. (2005). Membrane-proximal  $\alpha/\beta$  stalk interactions differentially regulate integrin activation. *J. Biol. Chem.* *280*, 24775–24783.
  47. Chen, Y., Lee, H., Tong, H., Schwartz, M., and Zhu, C. (2017). Force regulated conformational change of integrin  $\alpha V\beta_3$ . *Matrix Biol.* *60–61*, 70–85.
  48. Chen, Y., Li, Z., Kong, F., Ju, L.A., and Zhu, C. (2024). Force-regulated spontaneous conformational changes of integrins  $\alpha 5\beta 1$  and  $\alpha V\beta 3$ . *ACS Nano* *18*, 299–313. <https://doi.org/10.1021/acsnano.3c06253>.
  49. Chen, Y., Ju, L.A., Zhou, F., Liao, J., Xue, L., Su, Q.P., Jin, D., Yuan, Y., Lu, H., Jackson, S.P., and Zhu, C. (2019). An integrin  $\alpha IIb\beta_3$  intermediate affinity state mediates biomechanical platelet aggregation. *Nat. Mater.* *18*, 760–769.
  50. Chesla, S.E., Selvaraj, P., and Zhu, C. (1998). Measuring two-dimensional receptor-ligand binding kinetics by micropipette. *Biophys. J.* *75*, 1553–1572.
  51. Chen, W., Lou, J., Evans, E.A., and Zhu, C. (2012). Observing force-regulated conformational changes and ligand dissociation from a single integrin on cells. *J. Cell Biol.* *199*, 497–512.
  52. Campbell, I.D., and Humphries, M.J. (2011). Integrin structure, activation, and interactions. *Cold Spring Harb. Perspect. Biol.* *3*, a004994.
  53. Chen, W., Lou, J., Hsin, J., Schulten, K., Harvey, S.C., and Zhu, C. (2011). Molecular dynamics simulations of forced unbending of integrin  $\alpha V\beta_3$ . *PLoS Comput. Biol.* *7*, e1001086.
  54. Askari, J.A., Buckley, P.A., Mould, A.P., and Humphries, M.J. (2009). Linking integrin conformation to function. *J. Cell Sci.* *122*, 165–170.

55. Oakes, P.W., Bidone, T.C., Beckham, Y., Skeeters, A.V., Ramirez-San Juan, G.R., Winter, S.P., Voth, G.A., and Gardel, M.L. (2018). Lamellipodium is a myosin-independent mechanosensor. *Proc. Natl. Acad. Sci. USA* *115*, 2646–2651.
56. Lu, H., and Schulten, K. (2000). The key event in force-induced unfolding of titin's immunoglobulin domains. *Biophys. J.* *79*, 51–65.
57. Chen, Y., Liao, J., Yuan, Z., Li, K., Liu, B., Arnold Ju, L., and Zhu, C. (2019). Fast force loading disrupts molecular binding stability in human and mouse cell adhesions. *Mol. Cell. BioMech.* *16*, 211–223.
58. Li, Z., Delaney, M.K., O'Brien, K.A., and Du, X. (2010). Signaling during platelet adhesion and activation. *Arterioscler. Thromb. Vasc. Biol.* *30*, 2341–2349.
59. Mazzucato, M., Pradella, P., Cozzi, M.R., De Marco, L., and Ruggeri, Z.M. (2002). Sequential cytoplasmic calcium signals in a 2-stage platelet activation process induced by the glycoprotein  $Ib\alpha$  mechanoreceptor. *Blood* *100*, 2793–2800.
60. Nesbitt, W.S., Kulkarni, S., Giuliano, S., Goncalves, I., Dopheide, S.M., Yap, C.L., Harper, I.S., Salem, H.H., and Jackson, S.P. (2002). Distinct glycoprotein  $Ib/V/IX$  and integrin  $\alpha IIb\beta_3$ -dependent calcium signals cooperatively regulate platelet adhesion under flow. *J. Biol. Chem.* *277*, 2965–2972.
61. Kroll, M.H., Hellums, J.D., McIntire, L.V., Schafer, A.I., and Moake, J.L. (1996). Platelets and shear stress *88*, 1525–41. <https://pubmed.ncbi.nlm.nih.gov/8781407/>.
62. Xiong, J.-P., Mahalingam, B., Alonso, J.L., Borrelli, L.A., Rui, X., Anand, S., Hyman, B.T., Rysiok, T., Müller-Pompalla, D., Goodman, S.L., and Arnaout, M.A. (2009). Crystal structure of the complete integrin  $\alpha V\beta_3$  ectodomain plus an  $\alpha/\beta$  transmembrane fragment. *J. Cell Biol.* *186*, 589–600.
63. Xu, X.-P., Kim, E., Swift, M., Smith, J.W., Volkman, N., and Hanein, D. (2016). Three-dimensional structures of full-length, membrane-embedded human  $\alpha IIb\beta_3$  integrin complexes. *Biophys. J.* *110*, 798–809.
64. Van Der Spoel, D., Lindahl, E., Hess, B., Groenhof, G., Mark, A.E., and Berendsen, H.J.C. (2005). GROMACS: fast, flexible, and free. *J. Comput. Chem.* *26*, 1701–1718.
65. Schneider, C.A., Rasband, W.S., and Eliceiri, K.W. (2012). NIH Image to ImageJ: 25 years of image analysis. *Nat. Methods* *9*, 671–675.
66. Swift, M.L. (1997). GraphPad prism, data analysis, and scientific graphing. *J. Chem. Inf. Comput. Sci.* *37*, 411–412.
67. Humphrey, W., Dalke, A., and Schulten, K. (1996). VMD: visual molecular dynamics. *J. Mol. Graph.* *14*, 33.
68. Tan, S.K., Fong, K.P., Polizzi, N.F., Sternisha, A., Slusky, J.S.G., Yoon, K., DeGrado, W.F., and Bennett, J.S. (2019). Modulating integrin  $\alpha IIb\beta_3$  activity through mutagenesis of allosterically regulated intersubunit contacts. *Biochemistry* *58*, 3251–3259.
69. Bidone, T.C., Polley, A., Jin, J., Driscoll, T., Iwamoto, D.V., Calderwood, D.A., Schwartz, M.A., and Voth, G.A. (2019). Coarse-grained simulation of full-length integrin activation. *Biophys. J.* *116*, 1000–1010.
70. Fiser, A., Do, R.K.G., and Sali, A. (2000). Modeling of loops in protein structures. *Protein Sci.* *9*, 1753–1773.
71. Huang, J., and MacKerell, A.D., Jr. (2013). CHARMM36 all-atom additive protein force field: Validation based on comparison to NMR data. *J. Comput. Chem.* *34*, 2135–2145.
72. Lau, T.L., Kim, C., Ginsberg, M.H., and Ulmer, T.S. (2009). The structure of the integrin  $\alpha IIb\beta_3$  transmembrane complex explains integrin transmembrane signalling. *The EMBO journal* *28*, 1351–1361.
73. Meza, J.C. (2010). Steepest descent. *WIREs Computational Stats.* *2*, 719–722.
74. Hess, B., Bekker, H., Berendsen, H.J.C., and Fraaije, J.G.E.M. (1997). LINCS: A linear constraint solver for molecular simulations. *J. Comput. Chem.* *18*, 1463–1472.
75. Darden, T., York, D., and Pedersen, L. (1993). Particle mesh Ewald: An  $N \log(N)$  method for Ewald sums in large systems. *The Journal of chemical physics* *98*, 10089–10092.
76. Ke, Q., Gong, X., Liao, S., Duan, C., and Li, L. (2022). Effects of thermostats/barostats on physical properties of liquids by molecular dynamics simulations. *J. Mol. Liq.* *365*, 120116.
77. Wu, E.L., Cheng, X., Jo, S., Rui, H., Song, K.C., Dávila-Contreras, E.M., Qi, Y., Lee, J., Monje-Galvan, V., and Venable, R.M. (2014). CHARMM-GUI Membrane Builder toward Realistic Biological Membrane Simulations (Wiley Online Library).
78. Lau, T.-L., Dua, V., and Ulmer, T.S. (2008). Structure of the integrin  $\alpha IIb$  transmembrane segment. *J. Biol. Chem.* *283*, 16162–16168.
79. Jorgensen, W.L., Chandrasekhar, J., Madura, J.D., Impey, R.W., and Klein, M.L. (1983). Comparison of simple potential functions for simulating liquid water. *J. Chem. Phys.* *79*, 926–935.
80. Tekpinar, M., Neron, B., and Delarue, M. (2021). Extracting dynamical correlations and identifying key residues for allosteric communication in proteins by correlationplus. *J. Chem. Inf. Model.* *61*, 4832–4838.
81. Chen, Y., Liu, B., Ju, L., Hong, J., Ji, Q., Chen, W., and Zhu, C. (2015). Fluorescence Biomembrane Force Probe: Concurrent Quantitation of Receptor-ligand Kinetics and Binding-induced Intracellular Signaling on a Single Cell. *J. Vis. Exp.* e52975. <https://doi.org/10.3791/52975>.
82. Zhu, G., Zhang, Q., Reddy, E.C., Carrim, N., Chen, Y., Xu, X.R., Xu, M., Wang, Y., Hou, Y., Ma, L., et al. (2017). The integrin PSI domain has an endogenous thiol isomerase function and is a novel target for antiplatelet therapy. *Blood* *129*, 1840–1854. <https://doi.org/10.1182/blood-2016-07-729400>.

## STAR★METHODS

### KEY RESOURCES TABLE

REAGENT or RESOURCE	SOURCE	IDENTIFIER
<b>Antibodies</b>		
7H2 anti- $\beta_3$ integrin antibody	Developmental Studies Hybridoma Bank	RRID: AB_2617394
Alexa 488 conjugated secondary antibody	Thermo Fisher	Cat#A12379; RRID: AB_2759222
<b>Biological samples</b>		
Human red blood cells (RBCs) collected from human subjects (IRB Protocol #22- 0015)	This study	N/A
Platelets collected from human subjects (IRB Protocol #22- 0015)	This study	N/A
<b>Chemicals, peptides, and recombinant proteins</b>		
Fibrinogen	Sigma Aldrich	Cat#F4883
Biotin-PEG3500-NHS	JenKem USA	A5026-1
fibronectin type III module domains 9-10	A gift from Prof. Cheng Zhu (Georgia Tech) Chen et al. <sup>49</sup>	N/A
Streptavidin-maleimide	Sigma-Aldrich	S9415
Integrin $\alpha_{IIb}\beta_3$ purified from human platelets (IRB Protocol #22- 0015)	This study	N/A
<b>Critical commercial assays</b>		
BD FACSAria™ Fusion Cell Sorter	BD Bioscience	N/A
<b>Deposited data</b>		
Integrin $\alpha_v\beta_3$ headpiece	Xiong et al. <sup>62</sup>	PDB: 3IJE
Integrin $\alpha_{IIb}\beta_3$	Xu et al. <sup>63</sup>	N/A
Full-length structures of integrin $\alpha_v\beta_3$ and $\alpha_{IIb}\beta_3$ , MD simulation trajectories and analysis scripts	This study	<a href="https://github.com/tamarabidone/alphaV_vs_alphaIIb">https://github.com/tamarabidone/alphaV_vs_alphaIIb</a>
<b>Experimental models: Cell lines</b>		
CHO cells expressing $\alpha_{IIb}\beta_3$ or $\alpha_v\beta_3$	Joel Bennett & Karen Fong (Univ. of Pennsylvania)	N/A
<b>Software and algorithms</b>		
GROMACS (v2020)	Van Der Spoel et al. <sup>64</sup>	<a href="https://www.gromacs.org">https://www.gromacs.org</a>
ImageJ	Schneider et al. <sup>65</sup>	<a href="https://imagej.nih.gov/ij/">https://imagej.nih.gov/ij/</a>
GraphPad Prism	Swift et al. <sup>66</sup>	<a href="https://www.graphpad.com">https://www.graphpad.com</a>
VMD	Humphrey et al. <sup>67</sup>	<a href="https://www.ks.uiuc.edu/Research/vmd/">https://www.ks.uiuc.edu/Research/vmd/</a>
<b>Other</b>		
BD FACSAria™ Fusion gating strategy	BD FACSAria™ Fusion Flow Cytometer	N/A
Polyacrylamide gels of varying stiffness	Aratyn-Schaus et al. <sup>45</sup>	N/A

### EXPERIMENTAL MODEL AND STUDY PARTICIPANT DETAILS

#### Cell lines

CHO cells transfected with  $\alpha_{IIb}\beta_3$  or  $\alpha_v\beta_3$  were generously provided by Joel Bennett and Karen Fong (University of Pennsylvania).<sup>68</sup> Cells were cultured in Ham's F-12 medium containing 10% fetal bovine serum, 2 mM L-Glutamine, 100 units/ml Penicillin/Streptomycin, 300  $\mu$ g/mL Zeocin, and 500  $\mu$ g/mL G418 (Geneticin).

## METHOD DETAILS

### Cell culture and transfection

To obtain equal expression of  $\beta_3$  integrins, cells were FACS sorted (Figure S2) using antibody 7H2 (Developmental Studies Hybridoma Bank) to isolate cells with equivalent mid-level expressions of  $\alpha_{IIb}\beta_3$  and  $\alpha_V\beta_3$ . Flow cytometry was used to assess the cell surface expression levels of integrins  $\alpha_V\beta_3$  and  $\alpha_{IIb}\beta_3$  on CHO cells. Live cells were sequentially stained with the 7H2 primary antibody, which recognizes the  $\beta_3$  subunit of integrins and Alexa 488 conjugated secondary antibody for detection using the BD FACSAria Fusion Cell Sorter (BD Biosciences). Comparable expression levels of  $\beta_3$  subunit were observed across the populations. Gating strategies were applied to isolate distinct viable, single-cell populations. Representative plots show the gated populations (P1-P5 in Figure S2) with clear separation and high expression levels of  $\beta_3$  integrins. The histogram overlay further confirms uniform expression levels, as indicated by the similar intensity overlapping peaks (Figure S2E, J). The P4 and P5 populations exhibiting equivalent levels of  $\beta_3$  integrin expression were selected for further expansion. These populations were cultured under identical conditions, and ultimately, the P5 population (with mid-level expression) was chosen for downstream experiments due to its robust growth characteristics and stable expression profile. Cells were used at 5 or fewer passages after sorting.

### Substrate preparation

Polyacrylamide gels of varying stiffness were prepared as previously described. Briefly, a solution of 0.0714% glacial acetic acid, 0.0714% 3-(Trimethoxysilyl) propylmethacrylate, and 96% ethanol was applied to glass surfaces for 10 min. Polyacrylamide gels were prepared by combining 40% acrylamide, 2% bis-acrylamide, and citrate buffer supplemented with NHS, TEMED, and 10% APS, as specified by Table 1 for each stiffness. 20  $\mu$ L of the gel mix was swiftly added to each dish, and an 18 mm coverslip was gently placed on top to achieve uniform spreading. Polymerization occurred within 10 min, as indicated by a visible ring under the cover glass. After dislodging the coverslip, the gel was washed with citrate buffer and 1x PBS. Fibrinogen (20  $\mu$ L at 1 mg/mL) was added on top of the gel, incubated overnight at 4°C, and washed with PBS. Gels could be stored in 1x PBS for up to 2 weeks before use.

### Cell immunostaining and quantification

Cells were plated on polyacrylamide (PAA) substrates overnight then fixed with 4% paraformaldehyde (Electron Microscopy Sciences) in PBS. Fixed cells were permeabilized with 0.05% Triton X-100 in PBS supplemented with 320 mM sucrose and 6 mM MgCl<sub>2</sub>. Coverslips were washed with PBS 3X, blocked for 30 min with 1% BSA in PBS and incubated at room temperature for 1–2 h with phalloidin. After three PBS washes, cells were mounted with 4,6-diamidino-2-phenylindole (DAPI) in Fluoromount-G (SouthernBiotech) and images at 60x on a Nikon Eclipse Ti spinning disk confocal microscope. ImageJ was used for background subtraction, thresholding to generate cell masks, and analysis of particles function to determine cell area.<sup>65</sup>

### Reconstruction of missing residues

The bent  $\alpha_{IIb}\beta_3$  integrin, sourced from human platelets, was used.<sup>6,63</sup> For  $\alpha_V\beta_3$ , the full-length bent conformation was obtained by combining the headpiece (PDB: 3IJE) with the transmembrane helices and cytoplasmic domains (PDB: 2KNC) after structural fitting of their residues onto the corresponding regions of bent  $\alpha_{IIb}\beta_3$  integrin.<sup>62,69</sup> Missing residues, in both integrins, were reconstructed by considering residues within a 30 Å radius of the two terminal residues preceding the gap, using the loop modeling function in Modeller.<sup>70</sup> During the loop refinement process, all residues within this 30 Å radius were frozen, except for the terminal residues at either end of the gap. The reconstruction of the missing loops was optimized using the "refine.very\_slow" option. For each integrin type, 10,000 loop models were generated for each missing region, and the model with the lowest Modeller objective function was selected as the optimal structure. This refined model was then integrated into the original conformation. To ensure structural stability, the final conformation of each integrin underwent energy minimization using GROMACS.<sup>64</sup>

### All-atom molecular dynamics simulations of $\alpha_{IIb}\beta_3$ and $\alpha_V\beta_3$ extension and bending

To evaluate the degrees of extension (i.e., unbending) under force and bending (i.e., relaxation) of  $\alpha_{IIb}\beta_3$  and  $\alpha_V\beta_3$ , 100 ns of steered molecular dynamics (SMD) simulations were first performed, followed by 100 ns of equilibrium molecular dynamics (MD) simulations. All simulations were carried out in GROMACS,<sup>64</sup> using CHARMM36 force field,<sup>71</sup> and each simulation was repeated three times, resulting in three independent replicas for each integrin type. Structural analysis of integrin extension and bending was based on the degree of headpiece extension, changes in hydrogen bond numbers, and relative displacements of the extracellular functional domains.

### Energy minimization and equilibration steps

Bent integrin  $\alpha_{IIb}\beta_3$  ( $\alpha_V\beta_3$ ) was initially placed in a simulation box with dimensions of 16.1 nm  $\times$  13.1 nm  $\times$  22.9 nm (for  $\alpha_{IIb}\beta_3$ ) and 15.1 nm  $\times$  15.1 nm  $\times$  20.6 nm (for  $\alpha_V\beta_3$ ). The box size was then expanded in the direction of the applied force to more than double its original size, allowing sufficient space for the integrin's extension. Each integrin was solvated using the CHARMM-modified TIP3P water model and 150 mM NaCl.<sup>72</sup> The total number of atoms in  $\alpha_{IIb}\beta_3$  and  $\alpha_V\beta_3$  systems were 680,864 and 693,580, respectively. The solvated integrins were first subjected to energy minimization using the steepest descent algorithm for 5000 steps, with a timestep of 2 fs.<sup>73</sup> Covalent bonds involving hydrogen atoms were constrained using the LINCS algorithm.<sup>74</sup> Then, equilibration simulations were

performed using restraining potentials of backbone atoms (from 4000 kJ/mol/nm<sup>2</sup> to no restraints). First, two consecutive equilibration simulations were carried out in the constant temperature, constant volume (NVT) ensemble. Then, four successive equilibration simulations were run in the constant temperature and constant pressure (NPT) ensemble with a time step of 1 fs. The restraining potentials of the backbone atoms were gradually lowered during the consecutive equilibration runs. Using a switching function ranging from 1.0 to 1.2 nm, the Lennard-Jones interactions were cut off at 1.2 nm, and the short-range electrostatic cutoff was set at 1.2 nm. For the long-range electrostatic interactions, the particle-mesh Ewald approach was used<sup>75</sup> with a grid spacing of 0.16 nm.

### Steered molecular dynamics simulations and equilibrium molecular dynamics of $\alpha_{\text{IIB}}\beta_3$ and $\alpha_{\text{V}}\beta_3$ integrins

In production SMD (for extension) and equilibrium MD (for bending) simulations of both integrins, the control on pressure was turned off. A constant pulling force of 66.4 pN was applied on the center of geometry of the C $\alpha$  atoms forming the ligand binding site at the interface between  $\beta$ -propeller and  $\beta$ I domains (i.e., residues: E220, S121, S123, D119, D251 in the metal ion-dependent adhesion site, or MIDAS; D217, N215, D158, P219 in the ligand-associated metal ion binding site or LIMBS; and, D126, D127, M335 in the adjacent to MIDAS or ADMIDAS). The movement of the transmembrane helices was allowed laterally and constrained in the vertical direction to mimic restraints from the plasma membrane. A V-rescale thermostat was used to control the temperature<sup>76</sup>, and the LINCS algorithm was used to maintain the bond lengths.<sup>74</sup> Constant force pulling of the upper headpiece gradually unbent the integrin during SMD simulations without causing distortions of the domains (Videos S1). At 100 ns of SMD, the last frame of the SMD simulation was extracted and used as the first frame of equilibrium MD simulations to simulate the bending from the extended conformation. During the bending equilibrium MD simulations, the temperature was maintained at 310 K, and the pressure control was turned off, allowing the system to evolve naturally from the extended conformation. Visualization of the simulation trajectory was performed using VMD and Pymol.<sup>67</sup> GROMACS analysis tools and homemade scripts in Python were used to analyze the MD trajectories quantitatively.

### Membrane-embedded $\alpha_{\text{IIB}}\beta_3$ and $\alpha_{\text{V}}\beta_3$ simulations

The full-length all-atom structures of  $\alpha_{\text{IIB}}\beta_3$  and  $\alpha_{\text{V}}\beta_3$  integrins were also embedded in a lipid bilayer composed of DOPC and DOPS at a molar ratio of 4:1, using the CHARMM-GUI membrane builder (Figure S3A).<sup>77</sup> Both integrins were oriented so that their transmembrane  $\alpha$ -helices were perpendicular to the lipid bilayer.<sup>72,78</sup> The integrin-membrane systems were then solvated with the CHARMM-modified TIP3P water model.<sup>79</sup> The  $\alpha_{\text{IIB}}\beta_3$  ( $\alpha_{\text{V}}\beta_3$ ) system included 504 molecules of DOPC, 126 molecules of DOPS, 1077 (1017) sodium ions, 897 (841) chloride ions, and 323,037 (302555) water molecules (TIP3). The  $\alpha_{\text{IIB}}\beta_3$  ( $\alpha_{\text{V}}\beta_3$ ) system box size was 16.2 (16.2) nm, 16.2 (17) nm, and (50) 52 nm with a total number of 1084057 (1022865) atoms in each system. Energy minimization, equilibration (NVT and NPT ensembles), and production runs were performed as in the non-membrane simulations, using the same temperature conditions. Covalent bonds involving hydrogen atoms, and both short- and long-range interactions were handled in the same manner as in the non-membrane simulations.

### Structural and residue-based fluctuations analysis using RMSD and RMSF

Root-mean-square displacement (RMSD) analysis was used to assess the structural differences of each integrin during the simulations with respect to a reference (the first frame of the simulation, as shown in Figure 4A–B, or a conformation at a specific time in the simulations, as depicted in Figure 4F). RMSD was calculated as follows:

$$RMSD = \sqrt{\frac{1}{N} \sum_{i=1}^N \delta_i^2} \quad (\text{Equation 1})$$

where  $N$  is the number of C $\alpha$  atoms, and  $\delta_i$  is the distance between the  $i^{\text{th}}$  pair of corresponding atoms in the reference frame and the frame of interest from the MD trajectory.

Root-mean-square fluctuations (RMSF) analysis was used to assess the flexibility and fluctuations of individual residues within the integrin. Unlike RMSD, which provides a measure of the overall structural difference, RMSF offers a per-residue assessment by plotting the fluctuation values of each residue around its own average. RMSF is calculated as follows:

$$RMSF = \sqrt{\frac{1}{N} \sum_j (x_{ij} - \langle x_i \rangle)^2} \quad (\text{Equation 2})$$

where  $x_{ij}$  denotes the position of the  $i^{\text{th}}$  C $\alpha$  at the  $j^{\text{th}}$  frame, and  $\langle x_i \rangle$  is the averaged position of the  $i^{\text{th}}$  C $\alpha$  atom over the full trajectory.  $N$  is the total number of frames.

### Integrin residues motions analysis using Dynamic cross correlation

Dynamic cross correlation (DCC) maps were generated to analyze pairwise correlations between residues from the MD trajectories, using the CorrelationPlus package.<sup>80</sup> The DCC between residue pairs was calculated as:

$$C_{ij} = \frac{\langle \Delta r_i \cdot \Delta r_j \rangle}{\left( \sqrt{\langle \Delta r_i^2 \rangle} \cdot \sqrt{\langle \Delta r_j^2 \rangle} \right)} \quad (\text{Equation 3})$$

where  $\Delta r_i$  represents the displacement of residue  $i$  from its average position during the simulation. Positive  $C_{ij}$  values indicate correlated motion between residues  $i$  and  $j$ , meaning they move in the same direction or coordinate their movements. Negative  $C_{ij}$  values suggest anti-correlated motion, where residues  $i$  and  $j$  move in opposite directions or exhibit inversely related movements. A  $C_{ij}$  value of zero indicates no correlation between the motions of residues  $i$  and  $j$ .

### Biomembrane force probe setup, preparation, and experiment

All procedures involving human subjects were approved by the Institutional Review Board of The University of Texas Medical Branch (protocol number 22-0015).

### Red blood cell and glass bead preparation

Blood (8–10  $\mu$ L) from a human subject was obtained from finger prick. RBCs were isolated by centrifugation, biotinylated by incubating with Biotin-PEG3500-NHS solution and incubated with nystatin to reach the appropriate elasticity.<sup>47</sup>

For bead functionalization,<sup>81</sup> thiolated glass beads were incubated first with streptavidin-maleimide overnight and then with biotinylated fibronectin type III module domains 9–10 (FN<sub>III9–10</sub>) for another 3 h. All beads were finally washed with and resuspended in phosphate buffer (27.6 g/L NaH<sub>2</sub>PO<sub>4</sub>·H<sub>2</sub>O, 28.4 g/L Na<sub>2</sub>HPO<sub>4</sub>, pH 7.4).

### Platelet isolation

Blood was collected from healthy human adults into a syringe pre-loaded with ACD buffer (71 mM citric acid, 97 mM sodium citrate, 111 mM dextrose, pH 4.5) at a 5:1 ratio, added with 10  $\mu$ M Prostaglandin E<sub>1</sub> and centrifuged at 200 g for 15 min to isolate platelet rich plasma, which was centrifuged at 900 g for another 10 min to isolate the platelet pellet. The platelet pellet was resuspended in Modified Tyrode buffer (MTB) pH 6.5 (135 mM NaCl, 11.9 mM NaHCO<sub>3</sub>, 2.9 mM KCl, 0.42 mM NaH<sub>2</sub>PO<sub>4</sub>, 10 mM HEPES, 5.5 mM dextrose), added with 1.2 U/mL apyrase and 10  $\mu$ M Prostaglandin E<sub>1</sub>, and centrifuged again. Finally, the platelet pellet was resuspended into MTB pH 7.4 added with 1.2 U/mL apyrase.

### Biomembrane force probe setup, preparation and experiment

Our BFP setup has been described previously.<sup>81</sup> A chamber mounted on an inverted microscope (Olympus IX83) was filled with experimental buffer supplemented with 1% BSA and 1 mM Ca<sup>2+</sup>/Mg<sup>2+</sup>. An RBC was aspirated by a micropipette to act as a force transducer (Figure 6A, left), the spring constant of which was set to 0.3 pN/nm when assessing using >10-pN forces, and 0.2 pN/nm when using  $\leq$ 10-pN forces.<sup>47,48</sup> A probe bead bearing FN<sub>III9–10</sub> was attached to the apex of the RBC via streptavidin-biotin interaction. A bead functionalized by integrin  $\alpha_{IIb}\beta_3$  (purified from human plasma<sup>82</sup>) or a platelet was aspirated by an opposing micropipette (Figure 6A, right) as the target, and driven by a piezoelectric translator (Physical Instrument) to repeatedly touch with the probe bead and retract. The probe bead's position was tracked by a high-speed camera.

For observing integrin extension, the target bead/cell was first driven to approach and contact the probe bead and then retracted. A tensile force on the RBC, signified by the elongation of the RBC, would indicate an adhesion event. Coating of FN<sub>III9–10</sub> was titrated to maintain infrequent adhesion (<20%), which ensured that most (89%) of the adhesion events were mediated by a single integrin molecule.<sup>50</sup> Once an adhesion event was detected, the target bead/cell would be held at a pre-set position and clamped, until the adhesion event dissociated. The above procedure was repeated thousands of times on multiple target/probe pairs to acquire sufficient data. Data analyses were then performed on the BFP “force vs. time” signals of the repeated cycles, in which integrin extension events in the clamping phase were distinguished by a simultaneous drop of tensile force and thermal fluctuation level of the signal, which has been rigorously validated on integrins  $\alpha_v\beta_3$  and  $\alpha_L\beta_2$  by multiple works.<sup>47,48,50</sup> Control experiments were performed previously.<sup>49</sup> In this study, we employed the same instrumental setup and biological system. This approach ensured that the measured binding events were primarily driven by specific interactions between integrin  $\alpha_{IIb}\beta_3$  and its ligands,<sup>49</sup> with non-specific binding events and contributions from other integrins being negligible.

### QUANTIFICATION AND STATISTICAL ANALYSIS

Statistical details are provided in the figure legends and results section. Data are presented as means  $\pm$  SEM or s.d., with  $n$  indicating the number of cells or replicates. Statistical comparisons (e.g., t-tests) were used to evaluate differences between groups, with significance defined at  $p < 0.05$ . Figures 2B and 6 include statistical tests to assess differences in cell spread area and integrin unbending kinetics. Analyses were performed using standard software (e.g., GraphPad Prism), with sample sizes determined to ensure sufficient power.<sup>66</sup>